Modelling radiative properties of gas mixtures in nonequilibrium high-altitude rocket plumes

Timothee Guerra, Inigo Gonzalez de Arrieta, Olivier Rozenbaum, Cedric Blanchard

MODELLING RADIATIVE PROPERTIES OF GAS MIXTURES IN NONEQUILIBRIUM HIGH-ALTITUDE ROCKET PLUMES

G. Janodet,[1,2,3] Ph. Rivière,[1,*] J.-M. Lamet,[2] V. Rialland,[3] L. Tessé,[2] A. Soufiani[1]

[1] Laboratoire EM2C, CNRS CentraleSupélec Université Paris Saclay, Gif-sur-Yvette, 91192, France
[2] ONERA/DMPE, Université de Toulouse, Toulouse, 31000, France
[3] ONERA/DOTA, Université Paris-Saclay, Palaiseau, 91123, France

ABSTRACT. This paper presents the development of a Statistical Narrow Band model (SNB) in a nonequilibrium vibrational state for HCl and CO molecules. The population densities of the energy levels are obtained by a multi-temperature approach to compute nonequilibrium Line By Line (LBL) spectra. The SNB parameters are obtained by fitting the curves of growth from the LBL approach by a least squares error minimization using a Newton method for pure Lorentz and Doppler broadening regimes. The model is tested in Voigt broadening regime using a mixing rule and agrees well with the LBL approach. Finally, spectral correlation problems between $\eta_\sigma/\kappa_\sigma$ and κ_σ, where η_σ and κ_σ are the emission and absorption coefficients respectively, have been exhibited for $\mathrm{CO_2}$.

1. INTRODUCTION

The Local Thermodynamic Equilibrium (LTE) assumption is no longer valid when internal relaxation time scales are higher or comparable to hydrodynamic ones in gas flows. It can occur, for example, in high-altitude plumes when the flow undergoes a strong expansion at the nozzle exit. The gas is then under a Non-Local Thermodynamic Equilibrium (NLTE) state, which affects the molecule's radiative properties and thus needs to be considered for plume radiation [1]. However, using a high-resolution spectral approach to calculate the radiative properties makes solving the radiative transfer equation (RTE) too costly in the 3D coupled radiative-fluid computational framework.

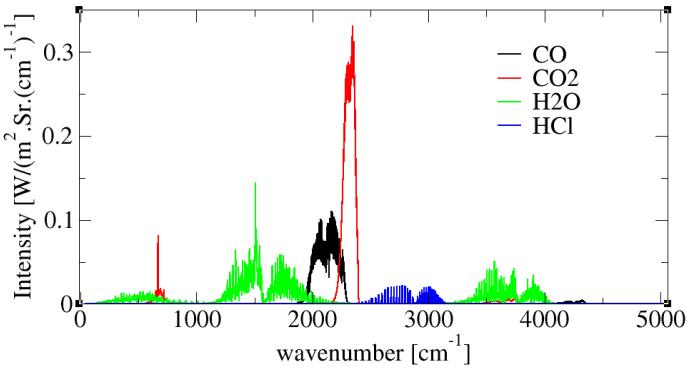

Figure 1. Radiation intensity emitted by a $10\ \mathrm{m}$ long column of exhaust gases at equilibrium with $T = 1000\ \mathrm{K}$, $p = 100\ \mathrm{Pa}$, and typical molar fractions $x_{H2O} = 0.0539$, $x_{CO2} = 0.0136$, $x_{CO} = 0.4397$, $x_{HCl} = 0.0191$. The high resolution intensities are averaged over $5\ \mathrm{cm^{-1}}$ for legibility reasons.

*Corresponding Ph. Rivière: philippe.riviere@centralesupelec.fr

This study investigates the radiative properties of gaseous species of high-altitude rocket engine plumes. In this case, the gaseous molecules that mainly contribute to radiation are CO_2 and H_2O. However, the spectral contributions of CO and HCl are not negligible, as shown in Fig. 1. In such expanding flows, CO_2, CO and HCl are in a nonequilibrium vibrational state [1]. For H_2O, the vibrational energy levels thermalize quickly with the translational levels and can therefore be modeled in the LTE assumption [2]. In this paper, nonequilibrium modeling of the radiative properties of CO, HCl and CO_2 molecules is considered, but only the SNB model for diatomic molecules is presented here.

2. SPECTROSCOPIC DATA AND MULTI-TEMPERATURE MODEL

The emission and absorption coefficients for wavenumber σ can be expressed under the assumption of independent lines as :

$$\eta_\sigma = \sum_{u\to l} \frac{A_{ul}}{4\pi} hc\sigma_{ul} n_u f_{ul}\left(\sigma - \sigma_{ul}\right), \tag{1}$$

$$\kappa_\sigma = \sum_{u\to l} \left(n_l B_{lu} - n_u B_{ul}\right) h\sigma_{ul} f_{ul}\left(\sigma - \sigma_{ul}\right), \tag{2}$$

where n_u and n_l are the populations of energy levels u and l of the radiating isotopologue, A_{ul}, B_{ul} and B_{lu} are the Einstein coefficients for spontaneous emission, induced emission, and absorption, σ_{ul} is the central transition wavenumber, and $f_{ul}(\sigma - \sigma_{ul})$ is the spectral line profile (assumed to be the same for the three radiative mechanisms) of the transition $u \to l$. Spectroscopic data were taken from HITEMP-2010 for CO_2 [3], HITEMP-2019 for CO [3] and HITRAN-2020 [4] for HCl. The population densities of the energy levels k are expressed using the multi-temperature approach and are defined as follows for the diatomic molecules [5] :

$$n_{k,\mathrm{HCl/CO}} = n_{\mathrm{HCl/CO}} Ab_I \frac{g_k}{Z_I\left(T, T_v\right)} \exp\left(-\frac{E^{rot}\{k\}}{k_B T} - \frac{E^{vib}\{k\}}{k_B T_v}\right), \tag{3}$$

where $n_{\mathrm{HCl/CO}}$ is the total population of HCl or CO respectively, Ab_I is the abundance of the isotopologue I considered, g_k is the degeneracy of level k. The partitioning scheme of the energy is composed of a rotational part $E^{rot}\{k\}$ and a vibrational part $E^{vib}\{k\}$ such as :

$$E^{vib}\{k\} = E^{vib}\{\boldsymbol{v_k}, J_k\} = \min_{J_k} E\{\boldsymbol{v_k}, J_k\}, \tag{4}$$

$$E^{rot}\{k\} = E\{\boldsymbol{v_k}, J_k\} - E^{vib}\{\boldsymbol{v_k}, J_k\}, \tag{5}$$

where $\boldsymbol{v_k}$ and J_k are the vibrational and rotational quantum numbers used for identifying the energy level k of energy $E\{\boldsymbol{v_k}, J_k\}$ in HITRAN/HITEMP spectroscopic databases. $Z_I(T, T_v)$ is the two-temperature partition function of the isotopologue I and its expression is

$$Z_I\left(T, T_\mathrm{v}\right) = \sum_k g_k \exp\left(-\frac{E^{rot}\{k\}}{k_B T} - \frac{E^{vib}\{k\}}{k_B T_v}\right). \tag{6}$$

For CO_2, the population of level k, using the three-temperature approach of [1], is given by

$$n_{k,\mathrm{CO_2}} = n_{\mathrm{CO_2}} Ab_I \frac{g_k}{Z_I\left(T, T_{12}, T_3\right)} \exp\left(-\frac{E^{rot}\{k\}}{k_B T} - \frac{E^{v_{12}}\{k\}}{k_B T_{12}} - \frac{E^{v_3}\{k\}}{k_B T_3}\right), \tag{7}$$

where T, T_{12}, T_3 are the temperature associated to, respectively, rotation-translation modes, coupled vibrational modes ν_1, ν_2 and antisymmetric vibrational mode ν_3. Details concerning the energy partitioning scheme ($E^{rot}\{k\}$, $E^{v12}\{k\}$, $E^{v3}\{k\}$) and the modelling of the three-temperature partition function Z_I may be found in [1].

The models and data presented in this section are used to perform LBL computations for HCl, CO, and $\mathrm{CO_2}$ molecules for the construction of SNB models. For diatomic molecules, a line wing cutoff of $500\ \mathrm{cm^{-1}}$ and a resolution of $10^{-2}\ \mathrm{cm^{-1}}$ were chosen for Lorentz profiles and $10\ \mathrm{cm^{-1}}$ and $10^{-3}\,\mathrm{cm^{-1}}$ respectively for Doppler profiles. For $\mathrm{CO_2}$, a line wing cutoff of $50\ \mathrm{cm^{-1}}$ and a resolution of $10^{-2}\ \mathrm{cm^{-1}}$ were selected for Lorentz profiles and $10\ \mathrm{cm^{-1}}$ and $10^{-3}\ \mathrm{cm^{-1}}$ respectively for Doppler profiles.

3. SNB MODEL FORMULATION FOR DIATOMIC MOLECULES

This section aims to develop a RTE formulation under nonequilibrium conditions suitable for applying statistical narrow-band models. The intensity escaping from a column (z_1, z_2), neglecting any incoming intensity in z_1, may be expressed as

$$I_\sigma(z_1 \to z_2) = \int_{z_1}^{z_2} \eta_\sigma(z)\tau_\sigma(z \to z_2)dz, \tag{8}$$

where $\tau_\sigma(z \to z_2) = \exp(-\int_z^{z_2} \kappa_\sigma(z)dz) = \dfrac{1}{\kappa_\sigma(z)}\dfrac{\partial \tau_\sigma}{\partial z}(z \to z_2)$ is the transmissivity of the column (z, z_2).

In order to use SNB models for solving the RTE, we need to express the intensity averaged over the spectral band $\Delta\sigma$. However, the emission coefficient η_σ and the transmissivity τ_σ are strongly correlated. To correctly account for self-correlation, the intensity averaged over the spectral band $\Delta\sigma$ is expressed as

$$\overline{I_\sigma}^{\Delta\sigma}(z_1 \to z_2) = \int_{z_1}^{z_2} \overline{\frac{\eta_\sigma}{\kappa_\sigma}(z)\frac{\partial \tau_\sigma}{\partial z}(z \to z_2)}^{\Delta\sigma} dz, \tag{9}$$

where $\dfrac{\eta_\sigma}{\kappa_\sigma}$ is the analog of Planck's function in LTE conditions.

To compute Eq.(9) with SNB models, a further simplification is necessary, which is

$$\overline{I_\sigma}^{\Delta\sigma}(z_1 \to z_2) \approx \int_{z_1}^{z_2} \overline{\left(\frac{\eta_\sigma}{\kappa_\sigma}(z)\right)}^{\Delta\sigma} \frac{\partial \overline{\tau_\sigma}^{\Delta\sigma}}{\partial z}(z \to z_2)dz, \tag{10}$$

assuming that $\dfrac{\eta_\sigma}{\kappa_\sigma}$ and $\dfrac{\partial \tau_\sigma}{\partial z}$ are not correlated. Under LTE conditions, this assumption is always true since Planck's function can be considered constant inside a narrow spectral band $\Delta\sigma$. The most critical test of this decorrelation assumption is to compare $\overline{\eta_\sigma}^{\Delta\sigma}$ with $\overline{\eta_\sigma/\kappa_\sigma}^{\Delta\sigma} \times \overline{\kappa_\sigma}^{\Delta\sigma}$. This comparison is performed for CO (Fig. 2) and for HCl (Fig. 3) and shows that $\dfrac{\eta_\sigma}{\kappa_\sigma}$ and κ_σ are perfectly decorrelated for significant nonequilibrium cases. The random SNB model of Mayer and Goody [6] has been selected in order to build an accurate model of mean transmissivities $\overline{\tau}^{\Delta\sigma}$. This model is based on statistical assumptions concerning line positions and intensities within a narrow band of width $\Delta\sigma$ and allows to express the transmissivity of a uniform column of length L, averaged over $\Delta\sigma$

$$\overline{\tau}^{\Delta\sigma}(L) = \frac{1}{\Delta\sigma}\int_{\Delta\sigma} \exp(-\kappa_\sigma L)d\sigma = \exp(-\frac{\overline{W}}{\delta}), \tag{11}$$

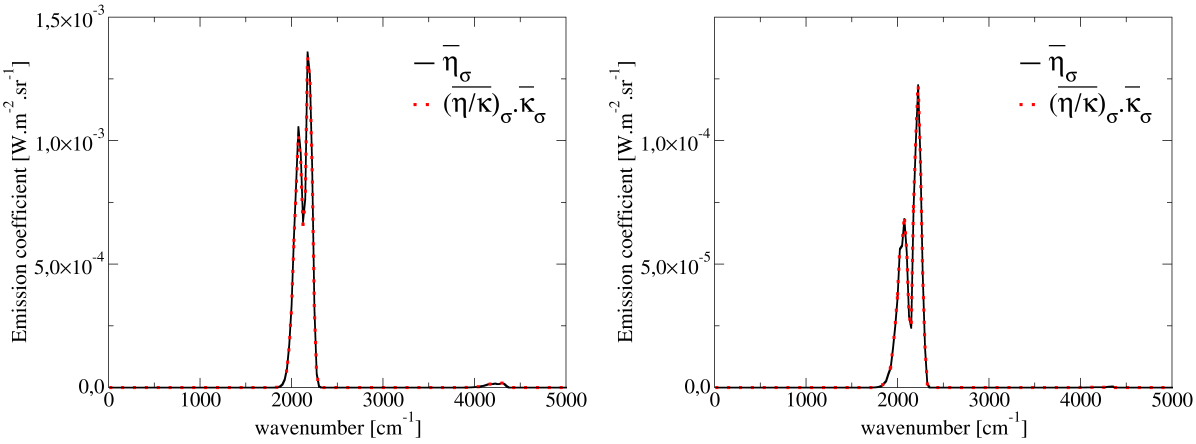

Figure 2. Comparison of $\overline{\eta_\sigma}^{\Delta\sigma}$ and $\overline{\eta_\sigma/\kappa_\sigma}^{\Delta\sigma} \times \overline{\kappa_\sigma}^{\Delta\sigma}$ for $x = 0.1$, $p = 100$ Pa, $T = 1000$ K, $T_v = 2000$ K (left) and $p = 100$ Pa, $T = 2000$ K, $T_v = 1000$ K (right) for CO

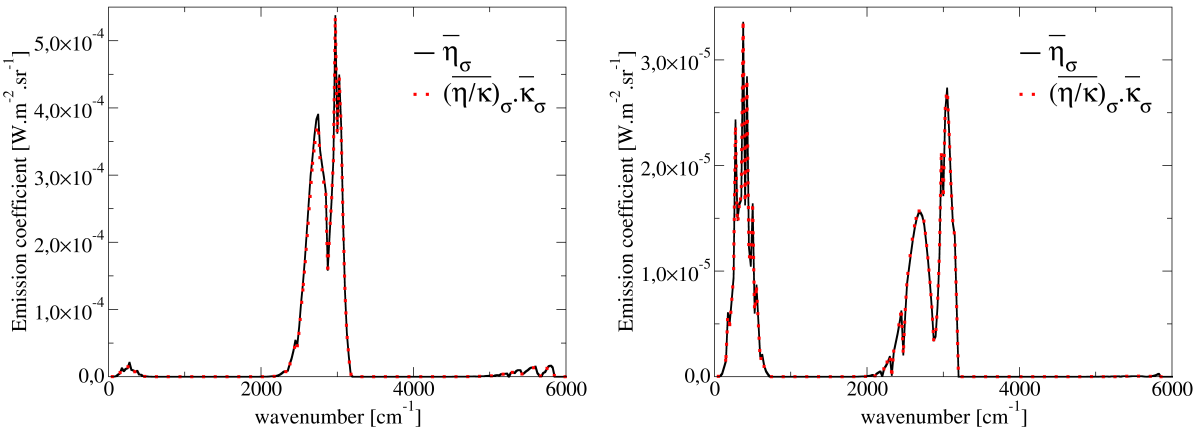

Figure 3. Comparison of $\overline{\eta_\sigma}^{\Delta\sigma}$ and $\overline{\eta_\sigma/\kappa_\sigma}^{\Delta\sigma} \times \overline{\kappa_\sigma}^{\Delta\sigma}$ for $x = 0.1$, $p = 100$ Pa, $T = 1000$ K, $T_v = 2000$ K (left) and $p = 100$ Pa, $T = 2000$ K, $T_v = 1000$ K (right) for HCl

with $\delta = \Delta\sigma/N$ the mean spacing between the N line positions within $\Delta\sigma$, and $\overline{W}$ the mean black equivalent width of these lines. Several line intensity distribution functions have been proposed to model $\overline{W}/\delta$ for Lorentz and Doppler line broadening. The most used ones are the Goody exponential distribution [6] and the Malkmus tailed inverse-exponential distribution [7]. They are special cases (respectively for $\alpha = -1$ et $\alpha = 0$) of the generalized Malkmus distribution function of [8].

$$P_\alpha(S) = \frac{C_\alpha}{S}\left(\frac{S_M}{S}\right)^\alpha \left[\exp\left(-\frac{S}{S_M}\right) - \exp\left(-\frac{rS}{S_M}\right)\right], \tag{12}$$

where C_α is a normalization constant.

In this study, we use the Malkmus distribution in the Lorentz broadening regime leading to

$$\frac{\overline{W_L}}{\delta} = \frac{2\overline{\gamma_L}}{\delta_L}\left(\sqrt{1 + \frac{\overline{k_L} xpL\overline{\delta_L}}{\overline{\gamma_L}}} - 1\right). \tag{13}$$

In the Doppler broadening regime, P_α distribution leads to the mean equivalent line width expression

$$\frac{\overline{W}_D}{\delta} = \overline{\beta_D} H_\alpha\left(\frac{\overline{k_D} xpL}{\overline{\beta_D}}\right), \tag{14}$$

with

$$H_\alpha(y) = \frac{1}{\alpha\sqrt{\pi}} \int_{-\infty}^{+\infty} [(1 + y\exp(-\xi^2))^\alpha - 1] d\xi \quad \text{for } \alpha \neq 0 \tag{15}$$

$$H_0(y) = \frac{1}{\sqrt{\pi}} \int_{-\infty}^{+\infty} \ln(1 + y\exp(-\xi^2)) d\xi \quad \text{for } \alpha = 0. \tag{16}$$

The parameters $\overline{k_L}$ and $\overline{k_D}$ are the reduced mean absorption coefficients and can be considered equal ($\overline{k_D} = \overline{k_L} = \overline{k} = \overline{\kappa}/(xp)$) with good accuracy in the significant spectral bands of the spectrum for radiative transfer, $\overline{\gamma_L}$ represents the mean Lorentz half width at half maximum of the lines, $\overline{\delta_L}$ is a modified mean line spacing, $\overline{\beta_D}$ characterizes the degree of line overlapping and x the molar fraction of the absorbing species.

For each broadening regime, parameters $\overline{k}$ have been obtained directly by averaging over each narrow band ($\Delta\sigma = 25\ \mathrm{cm}^{-1}$) high-resolution absorption coefficients provided by LBL calculations. The parameters $\overline{\delta_L}$ and $\overline{\beta_D}$ have been generated from adjustments enabling the corresponding analytical expression of $\overline{W_{L/D}/\delta}$, as a function of the column length L, fits the logarithm of the mean transmissivity obtained with LBL calculations (called the curve of growth). This adjustment is made by minimizing the least squares error on transmissivities thanks to the Newton method. The Lorentz half width at half maximum $\overline{\gamma_L}$ for CO has been taken from [9] and we used the estimated values from HITRAN-2020 for the coefficients of $\overline{\gamma_{L,\mathrm{HCl}}} = (p/p_s)\left[0.075 x_{\mathrm{HCl}}(T_s/T)^{0.92} + 0.011(1 - x_{\mathrm{HCl}})(T_s/T)^{0.5}\right]$. The parameters $\overline{\delta}_L$ and $\overline{k}$ are assumed independent of the pressure and are generated at $p = 1\mathrm{bar}$ for air-CO/HCl mixtures with $x = 0.1$. For the curve of growth adjustments in the Lorentz broadening regime, 20 transmissivities are prescribed from 0.02 to 0.95, and the associated column lengths are computed from these transmissivities. For the adjustments in Doppler broadening regime, 21 column lengths are provided from $xpL = 5$ Pa.m to $xpL = 5000$ Pa.m with a regular logarithmic step. To quantify the errors introduced by the SNB model, a mean quadratic error is defined as follows for each spectral band

$$s(\sigma) = \sqrt{\frac{1}{N_T.N_{T_v}.N_L}\left(\sum_{i=1}^{N_T}\sum_{j=1}^{N_{T_v}}\sum_{k=1}^{N_L}\left(\overline{\tau}^{\Delta\sigma}_{LBL}(\sigma, T_i, T_{v,j}, L_k) - \overline{\tau}^{\Delta\sigma}_{SNB}(\sigma, T_i, T_{v,j}, L_k)\right)^2\right)}, \tag{17}$$

where N_T, N_{T_v}, N_L are the number of points of the variable T, T_v, L respectively. This error estimator in both broadening regimes is presented in Fig. 4. and Fig. 5 for the diatomic molecules.

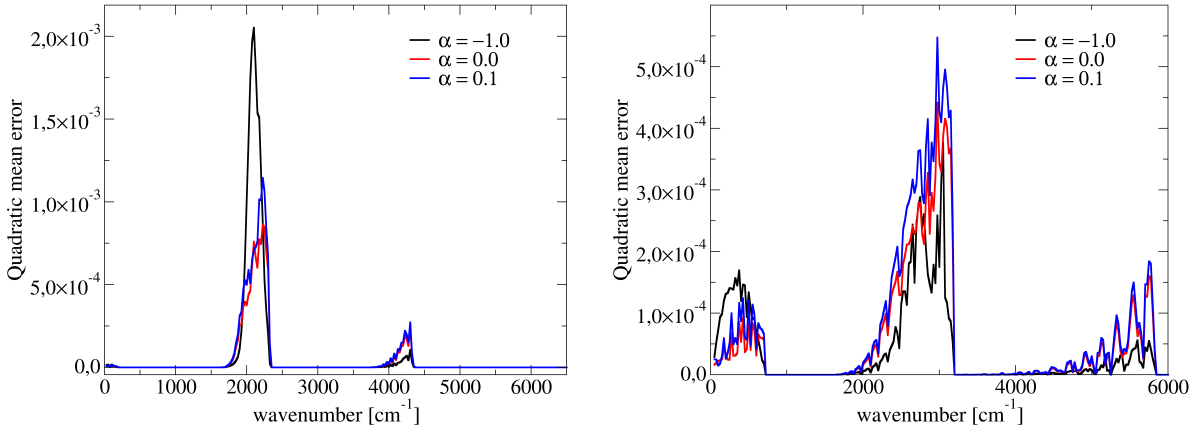

Figure 4. Quadratic mean error of the transmissivities in Doppler broadening regime along wavenumbers for CO (left) and HCl (right)

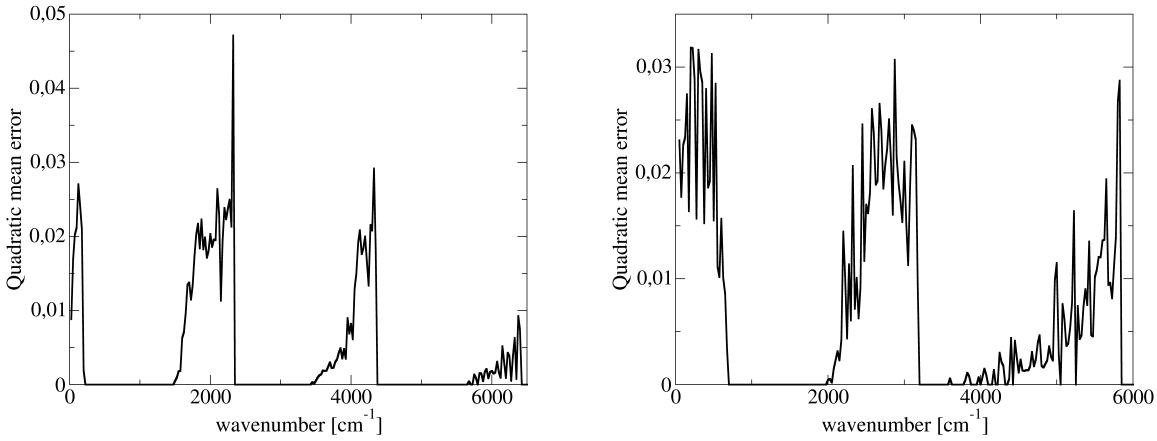

Figure 5. Quadratic mean error of the transmissivities in Lorentz broadening regime along wavenumbers for CO (left) and HCl (right)

For each molecule in the Doppler broadening regime, the α parameter was optimized by testing different values. It shows that the best α value on average across all temperature conditions is -1 for HCl and 0 for CO, which correspond to the exponential and the Malkmus distributions, respectively. The fit errors are maximum when performed in the molecule's absorption bands, which is expected since the curve of growth is linear for small optical thicknesses. The errors for Lorentz broadening regime appear higher than for the Doppler regime. However, transmissivities are prescribed in Lorentz broadening, which means that the adjustment is made for a wide range of optical thicknesses. Therefore, the errors displayed for Lorentz broadening involve an adjustment on all transmissivity ranges, unlike for Doppler broadening, where the adjustments are made on the optically thin or medium part of the curve of growth.

In the context of high-altitude rocket plumes, we have to consider the Voigt broadening regime for which the mean black equivalent line width is calculated by combining $\overline{W_L}/\delta$ and $\overline{W_D}/\delta$ expressions, according to

$$\frac{\overline{W_V}}{\delta} = \overline{k}xpL\sqrt{1-\Omega^{-1/2}} \quad \text{with}$$
$$\Omega = \left[1-\left(\frac{1}{\overline{k}xpL}\frac{\overline{W_D}}{\delta}\right)^2\right]^{-2} + \left[1-\left(\frac{1}{\overline{k}xpL}\frac{\overline{W_L}}{\delta}\right)^2\right]^{-2} - 1 \tag{18}$$

as proposed in [10].

To validate the SNB model in this regime, we compare the radiative intensity at the outlet of a uniform column of length $L = 1000\ \mathrm{m}$ from the model and the LBL approach in a wide range of pressure. This allows us to check the model in all broadening regimes and ensure that the mixing formula does not downgrade the model's accuracy. The comparison in Fig. 6 and Fig. 7 shows a good agreement between the SNB model and the LBL approach. Interestingly, the SNB model produces larger errors for the emitted radiative intensity in some band wings because the pressure-independent assumption of $\overline{k}$ is no longer valid in these spectral regions. Indeed, the reduced absorption coefficient $\overline{k}$ becomes proportional to the pressure in the band wings where the absorption coefficient is primarily due to far line wings. However, the contribution to the radiative transfer of these spectral bands is negligible, so these errors do not affect the relevance of the model.

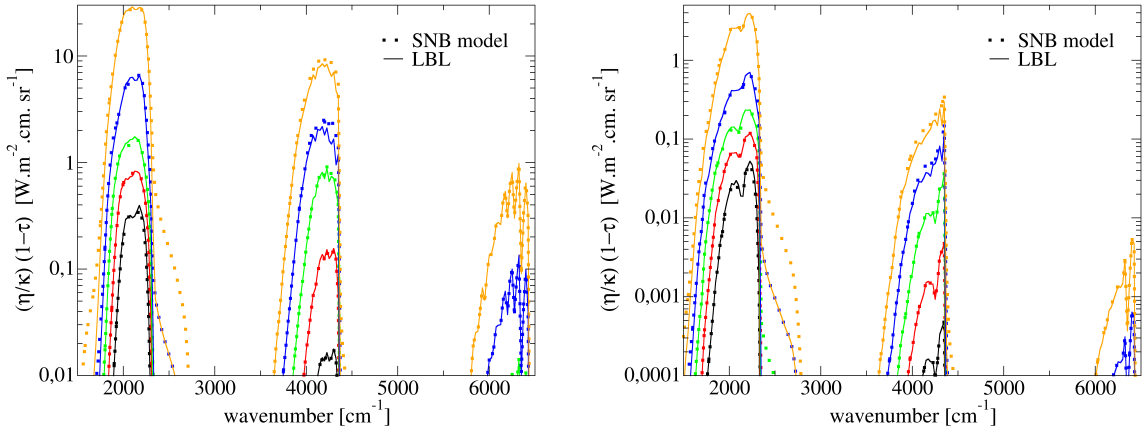

Figure 6. Radiative intensity for a uniform column at $L = 1000$ m for $x = 0.1$, $T = 1000$ K, $T_v = 2000$ K (left) and $T = 2000$ K, $T_v = 1000$ K (right) for CO. The pressures are 1 Pa (black), 10 Pa (red), 100 Pa (green), 1000 Pa (blue), 10000 Pa (yellow).

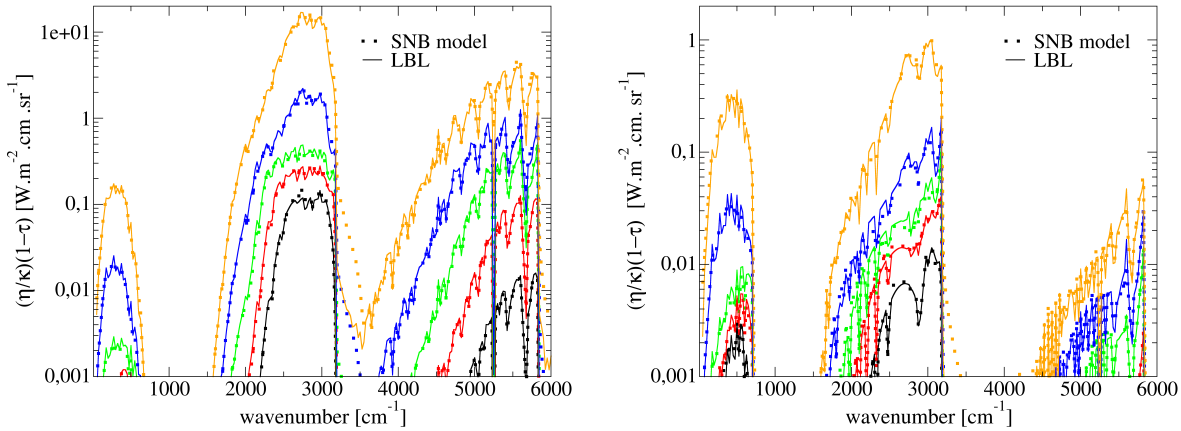

Figure 7. Radiative intensity for a uniform column at $L = 1000$ m for $x = 0.1$, $T = 1000$ K, $T_v = 2000$ K (left) and $T = 2000$ K, $T_v = 1000$ K (right) for HCl. The pressures are 1 Pa (black), 10 Pa (red), 100 Pa (green), 1000 Pa (blue), 10000 Pa (yellow).

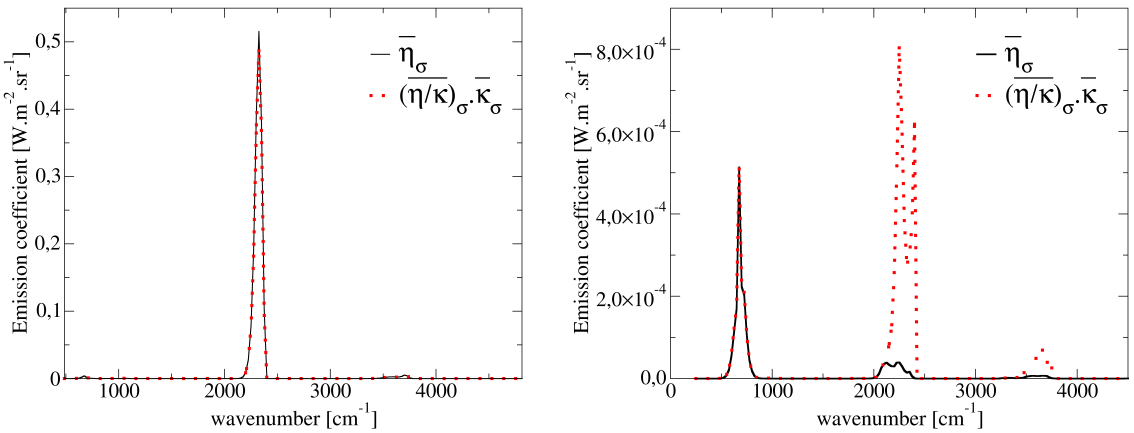

Figure 8. Spectral correlation tests for $x = 0.5$, $p = 100$ Pa, $T = 300$ K, $T_{12} = 1000$ K, $T_3 = 2000$ K (left) and $x = 0.5$, $P = 100$ Pa, $T = 2000$ K, $T_{12} = 1000$ K, $T_3 = 300$ K (right) for CO_2

4. SPECIFICITIES OF THE CO_2 MOLECULE

CO_2 molecule is characterized by three vibration modes ν_1, ν_2 and ν_3. The vibration temperature of the antisymmetric mode ν_3 can be in nonequilibrium with the coupled symmetric-transverse modes

ν_{12}. The multi-temperature model thus takes into account three temperatures instead of two for CO and HCl, which considerably increases the complexity of the spectral correlations between η_σ and κ_σ. The same decorrelation test in Voigt broadening regime, as shown in Fig. 2 and 3, was performed in Fig. 8 and showed an important correlation between $\eta_\sigma/\kappa_\sigma$ and κ_σ in the $2.7\mu\mathrm{m}$ and $4.3\mu\mathrm{m}$ bands for conditions where $T_{12} > T_3$ and $P < 1000$ Pa. To solve this issue, a vibrational splitting of the spectroscopic database is in progress and will be presented in future communication.

5. CONCLUSION

A nonequilibrium vibrational SNB model for CO and HCl has been developed and presented in this paper. The calculation of population densities for these diatomic molecules is based on a two-temperature approach (T, T_v). Since Kirchoff's law is no longer valid under these conditions, it is necessary to check the decorrelation between $\eta_\sigma/\kappa_\sigma$ and κ_σ beforehand. SNB model parameters were then obtained by adjusting the curves of growth obtained from the LBL approach for Lorentz and Doppler broadening regimes. The quality of the adjustments was then discussed quantitatively using error statistics. Finally, the SNB model was validated for the Voigt broadening regime by comparing the radiative intensity escaping from uniform columns for a wide range of pressures. For $\mathrm{CO_2}$, the calculation of population densities is based on a three-temperature approach (T, T_{12}, T_3). Nevertheless, unlike the diatomic molecules, decorrelation between $\eta_\sigma/\kappa_\sigma$ and κ_σ is no longer valid for crucial spectral bands. To overcome this issue, a vibrational splitting of the spectroscopic database is under development and will be presented in an incoming publication.

ACKNOWLEDGMENTS

The authors acknowledge the financial support of this study from the French Agence de l'Innovation de Défense (AID). This work was granted access to the HPC resources of IDRIS under the allocation 2022-A0102B00209 attributed by GENCI (Grand Equipement National de Calcul Intensif).

REFERENCES

[1] Q. Binauld and Ph. Rivière and J.M. Lamet and L.Tessé and A. Soufiani. $\mathrm{CO_2}$ IR radiation modelling with a multi-temperature approach in flows under vibrational nonequilibrium. *J. Quant, Spectrosc. Radiat. Transfer*, 239(106652), 2019.

[2] R. Taylor and S. Bitterman. Survey of vibrational relaxation data for processes important in the $\mathrm{CO_2} - \mathrm{N_2}$ laser system. *Reviews of Modern Physics*, 41(1):205,241,242, 1969.

[3] L. S. Rothman and I. E. Gordon et al. HITEMP, the high-temperature molecular spectroscopic database.

[4] I. E. Gordon and L. S. Rothman and R. J. Hargreaves et al. The HITRAN2020 molecular spectroscopic database. *J. Quant, Spectrosc. Radiat. Transfer*, 277(107949), 2022.

[5] E. Nagnibeda and E. Kustova. *Non-equilibrium reacting gas flows*. Springer, 2009.

[6] H.R. Goody and Y. Yung. *Atmospheric radiation*. Oxford University Press, 2nd edition, 1989.

[7] W. Malkmus. Random Lorentz Band Model with Exponential-Tailed S^{-1} Line-Intensity Distribution Function. *Journal of the Optical Society of America*, 57:323–329, 1967.

[8] Ph. Rivière and A. Soufiani. Generalized Malkmus line intensity distribution for $\mathrm{CO_2}$ infrared radiation in Doppler broadening regime. *Journal of Quantitative Spectroscopy and Radiative Transfer*, 112:475–485, 2011.

[9] Ph. Rivière and A. Soufiani. Updated band model parameters for $\mathrm{H_2O}$, $\mathrm{CO_2}$, $\mathrm{CH_4}$ and CO radiation at high temperature. *International Journal of Heat and Mass Transfer*, 55:3349–3358, 2012.

[10] C. Ludwig et al. *Handbook of infrared radiation from combustion gases*. Technical Report NASA SP-3080, 1973.